

Article

Heat and Mass Transfer Analysis of a Fluid Flow across the Conical Gap of a Cone-Disk Apparatus under the Thermophoretic Particles Motion

Pudhari Srilatha ¹, Srinivas Remidi ², Mulupuri Nagapavani ³ , Harjot Singh ⁴ and B. C. Prasannakumara ^{5,*} 

¹ Department of Mathematics, Institute of Aeronautical Engineering, Hyderabad 500043, Telangana, India

² Information Technology Department, College of Computing and Information Sciences, University of Technology and Applied Sciences-Nizwa, Nizwa 611, Oman

³ Department of Mathematics, Hyderabad Institute of Technology and Management, Hyderabad 501401, Telangana, India

⁴ Department of Mechanical Engineering, University Centre for Research & Development, Chandigarh University, Mohali 140413, Punjab, India

⁵ Department of Studies and Research in Mathematics, Davangere University, Davangere 577002, Karnataka, India

* Correspondence: prasannakumarabc@davangereuniversity.ac.in

Abstract: This particular study focuses on investigating the heat and mass transport characteristics of a liquid flow across the conical gap (CG) of a cone-disk apparatus (CDA). The cone and disk may be taken as stationary or rotating at varying angular velocities. Consideration is given to heat transport affected by solar radiation. The Rosseland approximation is used for heat radiation calculations in the current work. To observe the mass deposition variation on the surface, the effect of thermophoresis is taken into account. Appropriate similarity transformations are used to convert the three-dimensional boundary-layer governing partial differential equations (PDEs) into a nonlinear ordinary differential equations (ODEs) system. Particularly for the flow, thermal and concentration profiles, plots are provided and examined. Results reveal that the flow field upsurges significantly with upward values of Reynolds numbers for both cone and disk rotations. The increase in values of the radiation parameter improves heat transport. Moreover, it is detected that the stationary cone and rotating disk model shows improved heat transport for an increase in the values of the radiation parameter.

Keywords: cone-disk apparatus; thermophoresis; conical gap; thermal radiation; heat and mass transfer



Citation: Srilatha, P.; Remidi, S.; Nagapavani, M.; Singh, H.; Prasannakumara, B.C. Heat and Mass Transfer Analysis of a Fluid Flow across the Conical Gap of a Cone-Disk Apparatus under the Thermophoretic Particles Motion. *Energies* **2023**, *16*, 952. <https://doi.org/10.3390/en16020952>

Academic Editor: Dmitry Eskin

Received: 26 November 2022

Revised: 31 December 2022

Accepted: 8 January 2023

Published: 14 January 2023



Copyright: © 2023 by the authors. Licensee MDPI, Basel, Switzerland. This article is an open access article distributed under the terms and conditions of the Creative Commons Attribution (CC BY) license (<https://creativecommons.org/licenses/by/4.0/>).

1. Introduction

The cone-disk apparatus (CDA) has several applications, such as the stability scrutiny of the creeping flow of Oldroyd-B liquid [1], fluid viscosity estimation [2], and applications of bioengineering for propagating endothelium cells placed as a monolayer on the plate [3]. Cone-disk devices, where liquid flow occurs in a CG at angles of 1 to 5 degrees. The current research also focuses on the flow, mass, and heat passage in the CG between a CDA, co-counter rotating or both stationary at varied angular speeds. Shevchuk [4] was initially provided the self-similar versions of energy and Navier–Stokes equations (NSEs) for a heat transport and laminar flow in a CDA. The flow of the nanofluid (NF) was studied by Basavarajappa and Bhatta [5] in a CDA by pondering the suitable rotational Reynolds numbers and Buongiorno model. Wang et al. [6] scrutinized the impact of radiation on the NF flow among the CG of a CDA. Here, their research suggests that for higher values of the radiation parameter, the dynamics of flow with nanoparticle aggregation instance exhibits better-quality heat transmission. From the perspective of the stabilization of thermal energy, Alrabaiah et al. [7] addressed the microbes-based flow of hybrid NF using the CDA. Here, they discovered that, while the temperature at the outside edge is static, a circulating disk and a stationary cone may effectively cool the CDA. The flow of the hybrid NF in the conical space of CDA was examined by Gul et al. [8]. They stated that, for a revolving disk

with a stationary cone, the required cooling of CDA may be achieved while the surface temperature stays constant.

A phenomenon of small-particle migration in the direction of a reducing thermal gradient is known as thermophoresis. The force felt by the suspended particle is referred to as thermophoretic force, and the velocity the particle acquires is referred to as thermophoretic velocity [9–11]. Small particles accumulate on the cold surfaces as a result of thermophoresis. Gowda et al. [12] explored the thermophoretic particle deposition (TPD) in unsteady hybrid NF flow over a revolving disk. According to their results, an increase in thermophoretic coefficient and parameter values causes a decrease in the mass transfer rate. Khan et al. [13] examined the interaction between TPD and the radiation effect along a stretched sheet in a two-dimensional thin-film stream of second-grade liquid. The TPD impact on the Glauert wall jet slip flow of NF was induced by Alhadhrami et al. [14]. Their results indicate that an increase in the heat transfer rate may be achieved by increasing the values of the radiation parameter and volume fraction simultaneously. Increasing the values of the thermophoretic parameter results in an increase in the rate of mass transfer. Abbas et al. [15] explored the combination of TPD and radiation effects on the convective flow of optically dense gray fluid. Using the TPD, Shah et al. [16] analyzed the effect of convective heating on the second-grade fluid flow past an upright surface.

The heat and mass transport over the surface of a rotating disk with the fluid flow has attracted a considerable amount of consideration from researchers. Owing to the fact that it has several applications in technical and aerospace sciences, including thermal energy-producing systems, rotational equipment, steam turbine deltoids, the geothermal sector, and medical equipment. Karman [17], in his paper on the solution of NSEs by making use of the proper transformation, presented the concept of liquid flow across a rotating system for the very first time. Turkyilmazoglu [18] examined flow and heat transport using CDA. Shevchuk [19] studied the laminar heat and mass transference in a CDA. The flow of an NF caused by a revolving disk was studied by Tassaddiq et al. [20]. Turkyilmazoglu and Senel [21] conferred the heat and mass transference of the flow that occurred across a spinning, porous disk.

Thermal radiation is significant in satellites, aircraft missiles, gas turbines, spacecraft, and nuclear power plants. Shevchuk [22] investigated the effect of radiation on a self-similar solution across spinning CDA. The effects of heat radiation on NF flow were inspected by Kumar et al. [23]. Their results indicate that an increase in the values of the radiation parameter produces an improvement in the thermal profile as a result of the generation of internal heat. Kumar et al. [24] analyzed magnetic liquid flow when heat radiation occurred from an stretched sheet. In this study, the researchers primarily concentrate on a magnetic fluid that is electrically non-conducting, incompressible, which has a modest saturation magnetization, and has a low Curie temperature. Alzahrani et al. [25] investigated the effect of radiation on the plane wall jet flow of Casson NF. In this study, the researchers conclude that an increase in the Casson parameter's value would result in a decrease in the heat transfer rate assumed for nanoliquids, while an increase in the radiation parameter's value would show the opposite tendency. Jayaprakash et al. [26] conferred the impact of heat radiation on the NF flow past a sheet. They concluded that an improvement in the heat transfer process may be observed for increased levels of radiation and ferromagnetic interaction parameters.

The abovementioned studies show that no effort has been made to date to scrutinize the impact of TPD on the three-dimensional flow of fluid by considering the radiation effect concerning the disk and cone as moving or stationary, under the influence of thermal radiation. The main priority is to extend the idea of Refs. [5,18], which also consist of the most relevant studies related to the present model, and to develop a mathematical model for the rotating disk and cone, which are considered as moving or stationary, in both cases counter-rotating or co-rotating. Furthermore, a visual representation of the numerical outcomes are presented and discussed. The purpose of this study is to analyze the non-dimensional parameters that affect flow, heat, and mass transfer processes.

2. Mathematical Formulation

The conical gap between a cone and disk was considered, which was filled with an incompressible viscous fluid. The velocity components (u, v, w) were considered along (r, φ, z) an increasing direction. The axisymmetric flow assumption eliminated tangential component derivatives. It was assumed that both tools were either fixed or rotating at varying angular velocities, as indicated in Figure 1. There was a total of four distinct physical configurations that were considered, (i) including a rotating cone with static disk, (ii) static cone with rotating disk, (iii) the co-rotation of disk and cone, and (iv) counter-rotation of disk and cone (see Refs. [8,18,19]).

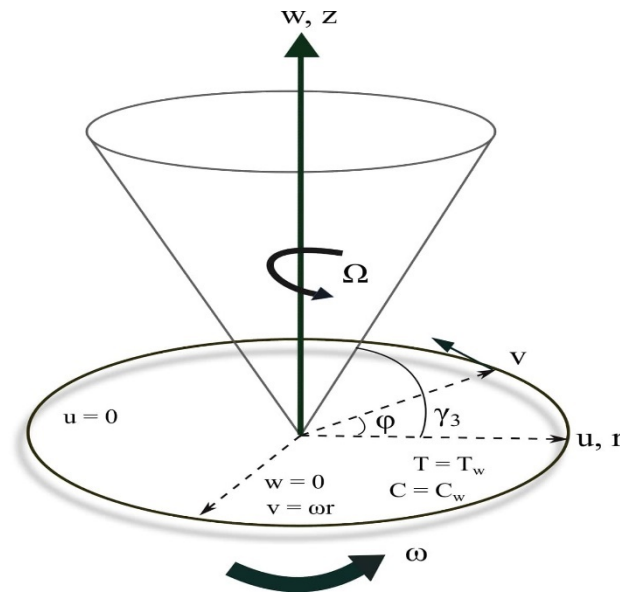


Figure 1. Geometry of the conical gap flow between a cone and disc. The diagram of the flow of fluid is depicted for the case of a rotating cone and disc with the velocity components (u, v, w) along the (r, φ, z) direction.

The generalized mathematical model, which is presented as follows:

$$\nabla \cdot \vec{u} = 0, \tag{1}$$

Equation (1) is the continuity equation that shows that the in-flow equals the out-flow. The conservation of momentum is the following:

$$\rho_f((\vec{u} \cdot \nabla) \vec{u}) = -\nabla p + \mu_f \nabla^2 \vec{u}, \tag{2}$$

Equation (2) is the momentum equation that represents the conservation law of momentum. The symbols on the left-hand side of Equation (2) result from inertial forces, the first term on the right-hand side is due to the pressure force, and the second term is due to viscous forces.

The conservation of energy is:

$$(\rho C_p)_f((\vec{u} \cdot \nabla) T) = k_f \nabla^2 T, \tag{3}$$

the conservation of the nanoparticles volume fraction is:

$$((\vec{u} \cdot \nabla) C) = D_f \nabla^2 C. \tag{4}$$

Consideration is given to heat transport affected by solar radiation. The Rosseland approximation was used for heat radiation calculations in the current study. Equation (3) takes the following form:

$$\left(u \frac{\partial T}{\partial r} + w \frac{\partial T}{\partial z}\right) = \frac{k_f}{(\rho C_p)_f} \left(\frac{\partial^2 T}{\partial r^2} + \frac{1}{r} \frac{\partial T}{\partial r} + \frac{\partial^2 T}{\partial z^2}\right) + \frac{16\sigma^* T_\infty^3}{(\rho C_p)_f 3k^*} \left(\frac{\partial^2 T}{\partial r^2} + \frac{1}{r} \frac{\partial T}{\partial r} + \frac{\partial^2 T}{\partial z^2}\right), \quad (5)$$

Equation (5) represents the conservation law of energy. Here, the last term on the right-hand side shows the additional effect of thermal radiation. To observe the variation in mass deposition on the surface, the effect of TPD was considered. The particle mass flux was negligible to prevent thermophysical processes from having an influence on the main stream speed and temperature field. Because of its low concentration, the particle's surface concentration was zero. The particles were absorbed by the surface after impact and did not bounce back. Here, Equation (4) takes the following form:

$$\left(u \frac{\partial C}{\partial r} + w \frac{\partial C}{\partial z}\right) = D_f \left(\frac{\partial^2 C}{\partial r^2} + \frac{1}{r} \frac{\partial C}{\partial r} + \frac{\partial^2 C}{\partial z^2}\right) - \frac{\partial}{\partial z}(CW_T) \quad (6)$$

The boundary conditions are:

$$\left. \begin{aligned} (u, v, w, T) &= (0, \omega r, 0, T_w), C = C_w = 0 \text{ (fully absorbing and clean surface) at } z = 0, \\ (u, v, w, T, C) &= (0, \Omega r, 0, T_\infty, C_\infty) \text{ at } z = r \tan \gamma. \end{aligned} \right\} \quad (7)$$

The impacts of thermophoresis are accounted to observe mass deposition alternation on surface. The main stream speed and temperature field are unaffected by thermophysical processes because particles mass flux is reasonably small. Only the thermophoretic velocity component that is normal to the surface is significant because the thermal gradient in the z-direction is much greater than that in the r-direction due to the behavior of the boundary layer. The thermophoretic deposition velocity in the z-direction is presented by (see Refs. [27–30])

$$W_T = -\frac{\nu_f k^*}{T} \left(\frac{\partial T}{\partial z}\right) \quad (8)$$

We remark that only the velocity component presented by (8) is to be considered within the boundary-layer assumptions.

Where the thermophoretic co-efficient k^* can take on any value between 0.2 and 1.2.

The similarity variables can be illustrated in the following manner (see Refs. [8,18,19]):

$$u = \frac{\nu_f F}{r}, C = \chi C_\infty, T = T_\infty + \theta(T_w - T_\infty), w = \frac{\nu_f H}{r}, v = \frac{\nu_f G}{r}, \eta = \frac{z}{r}, p = \frac{\rho_f \nu_f^2}{r^2} P.$$

which reduces Equations (1)–(7) as follows:

$$H' - \eta F' = 0 \quad (9)$$

$$(1 + \eta^2)F'' + 3\eta F' + F(\eta F' + F) - HF' + G^2 + 2P + \eta P' = 0, \quad (10)$$

$$(1 + \eta^2)G'' + 3\eta G' + \eta FG' - HG' = 0, \quad (11)$$

$$(1 + \eta^2)H'' + 3\eta H' + H - P' + FH + \eta FH' - HH' = 0, \quad (12)$$

$$\frac{1}{\text{Pr}}(1 + R)(\eta\theta' + (1 + \eta^2)\theta'') + \eta\theta'F - H\theta' = 0, \quad (13)$$

$$\left. \frac{1}{\text{Sc}}(\eta\chi' + (1 + \eta^2)\chi'') + \eta\chi'F - H\chi' + k^* N_t(1 - N_t\theta)^{-1}(\theta''\chi - N_t(1 - N_t\theta)^{-1}\theta'^2\chi + \theta'\chi') = 0. \right\} \quad (14)$$

The modified boundary constraints are as follows:

$$\left. \begin{aligned} F(0) = 0, G(0) = \text{Re}_\omega, H(0) = 0, \theta(0) = 1, \chi(0) = 0, \\ F(\eta_0) = 0, H(\eta_0) = 0, G(\eta_0) = \text{Re}_\Omega, \theta(\eta_0) = 0, \chi(\eta_0) = 1. \end{aligned} \right\} \quad (15)$$

The following is a list of dimensionless parameters for the proposed study:

$$\text{Re}_\omega = \frac{r^2\omega}{\nu_f}, Sc = \frac{\nu_f}{D_f}, N_t = \frac{T_\infty - T_w}{T_\infty}, R = \frac{16\sigma^* T_\infty^3}{3k^* k_f}, \text{Pr} = \frac{\mu_f C_p}{k_f}, \text{Re}_\Omega = \frac{r^2\Omega}{\nu_f}. \quad (16)$$

The skin-friction coefficients at the disk surface are as follows (see Ref. [5]):

$$\text{tangential skin - friction} = G'(0), \quad (17)$$

$$\text{radial skin - friction} = F'(0). \quad (18)$$

The heat transfer occurring at the surface of the cone and disk are as follows (see Refs. [5,6]):

$$Nu_d = -(1 + R)\theta'(0), Nu_c = -(1 + R)\theta'(\eta_0). \quad (19)$$

$$Sh_d = -\chi'(0), Sh_c = -\chi'(\eta_0). \quad (20)$$

3. Numerical Procedure

The shooting approach was used to numerically solve the system of nonlinear ODEs (Equations (9)–(14)) and the boundary conditions (Equation (15)). Initially, first-order differential equations were used to solve the two-point boundary value issue (initial value problem). Additionally, a shooting technique was used to predict the initial conditions that were missed. Later, the resulting one was integrated using the RKF-45 approach (see Refs. [23–26]). Here, a fifth-order Runge–Kutta technique was used together with a fourth-order Runge–Kutta procedure. Subtracting these two numbers reveals the algorithm's error, which can then be used to determine the appropriate step size. The RKF-45 process algorithm is as follows:

$$\begin{aligned} k_0 &= F(x_k, y_k), \\ k_1 &= F\left(x_k + \frac{1}{4}h, y_k + \frac{1}{4}k_0\right), \\ k_2 &= F\left(x_k + \frac{3}{8}h, y_k + h\left[\frac{3}{32}k_0 + \frac{9}{32}k_1\right]\right), \\ k_3 &= F\left(x_k + \frac{12h}{13}, y_k + h\left(\frac{1932k_0}{2197} - \frac{7200k_1}{2197} + \frac{7296k_2}{2197}\right)\right), \\ k_4 &= F\left(x_k + h, y_k + h\left[\frac{439k_0}{216} - 8k_1 + \frac{3680k_2}{513} - \frac{845}{4104}k_3\right]\right), \\ k_5 &= F\left(x_k + \frac{h}{2}, y_k - \frac{8h}{27}k_0 + 2hk_1 - \frac{3544}{2565}hk_2 + \frac{1859}{4104}hk_3 - \frac{11}{40}hk_4\right). \\ y_{k+1} &= y_k + \frac{25}{216}hk_0 + \frac{1408}{2565}hk_2 + \frac{2197}{4109}hk_3 - \frac{1}{5}hk_4, \\ y_{k+1} &= y_k + \frac{16}{135}hk_0 + \frac{6656}{12825}hk_2 + \frac{28561}{56430}hk_3 - \frac{9}{50}hk_4 + \frac{2}{55}hk_5. \end{aligned}$$

The problem domain was considered as $[0, \eta_{max}]$ in the calculations, where η_{max} . The step size was carefully selected as $\Delta\eta = 0.001$. An assessment of the RKF procedure using the shooting method and bvp4c is graphically presented to further explain the verification of the utilized model. With the aid of MATLAB software, the numerical results were obtained, and the numerical results were validated against previously published work. Additionally, the numerical results of the present study were compared to earlier studies, and the outcomes agreed with one another (see Tables 1 and 2). We repeated the method with several parameter values to fully verify the results of the suggested model.

Table 1. Comparison of the current study’s coefficient of heat transfer rate when R = 0.

Models	Re	Shevchuk [19]	Turkylmazoglu [18]	Basavarajappa and Bhatta [5]	Present Results
I. Rotating cone with a stationary disk.	2463	13.401	13.4006970	13.40069715	13.40069716
	12	0.954	0.95405487	0.95405477	0.954054771
II. Stationary cone with a rotating disk.	2463	15.353	15.3528734	15.35287341	15.35287342
	12	1.041	1.04080471	1.04080467	1.040804672
III. Co-rotating cone and disk.	2463	14.346	14.3466439	14.34664704	14.34664705
	12	1.001	1.00087052	1.00087491	1.000874913
IV. Counter-rotating cone and disk.	2463	14.440	14.4395241	14.43952407	14.43952409
	12	0.989	0.98884832	0.98884832	0.988848323

Table 2. Comparison of the current study with previous research for a few limited cases.

Models		Turkylmazoglu [18]	Basavarajappa and Bhatta [5]	Present Results
I	Nu_c	0.83028093	0.83028103	0.83028104
	Nu_d	1.09328442	1.09328437	1.09328437
II	Nu_c	0.78069847	0.78069848	0.78069849
	Nu_d	1.17198527	1.17198529	1.17198530
III	Nu_c	0.80178312	0.80177021	0.80177022
	Nu_d	1.13538224	1.13540222	1.13540222
IV	Nu_c	0.81339331	0.81339331	0.81339332
	Nu_d	1.12618149	1.12618149	1.12618150

4. Results and Discussion

This section presents a detailed observation of the impact of dimensionless parameters on velocity, temperature, and concentration fields. Here, the computations to Reynolds numbers were restricted to 12 corresponding to the gap angle $\pi/45$ representing a flow configuration with a small gap. In the event of co-gyrating, the ratio of Reynolds numbers was set to 12, whereas in the case of counter-gyrating, it was set to -12 . Throughout the calculations, some of the parameters’ values were fixed as $Pr = 7$, $k^*0.5$, $R = 0.5$, $N_t = 0.1, Sc = 2.5$, $Re_\omega = 1$, $Re_\Omega = 2$. The values of these parameters did not change, unless they are shown in the graphs and tables.

Figure 2a–d exhibits the influence of Reynolds numbers on $G(\eta)$ for all four models mentioned above. The scenarios for what time the disk was at rest and the revolving cone are shown in Figure 2a. Between the spaces in the disk and cone, the fluid flows. A positive change in cone velocity values improved the velocity profile $G(\eta)$, although the greatest flow intensity was located around the cone. The flow field presented in Figure 2b,d exhibits its supremacy over Re_Ω and Re_ω , since both the surfaces spin in the same direction and encounter the least resistance. Figure 2c illustrates how, with the least amount of resistance, the co-gyration of the disk and cone efficiently enhances the fluid velocity.

Figure 3a–d shows the effect of R on $\theta(\eta)$ four different models. Here, the escalation in values of R improves $\theta(\eta)$ for all four cases. The radiation parameter $R = \frac{16\sigma^*T_\infty^3}{3k^*k_f}$ in the energy Equation (20) is demarcated as the ratio of radiation heat contribution relative to thermal conduction. Strengthening the fluid’s thermal diffusivity and accelerating the thermal energy inside the related layer are the effects of increasing the thermal radiation contribution with an increase in R . As a result, as illustrated in the figures, $\theta(\eta)$ increases with an upsurge in R . From Figure 3a–d, it is detected that the stationary cone and rotating disk model shows improved heat transport for an increase in values of R . Figures 4a–d and 5a–d show the impact of N_t and k^* on mass transport, respectively, for four different models. Here, the increase in values of both N_t and k^* declines the mass transport activity in all four cases. According to Figure 4a–d, the mass transport field for N_t decreases as the temperature ratios increase because the thermophoretic force causes more particles to approach the apparatus at higher temperatures, which reduces the con-

centration further from the cool surface. The concentration profiles decrease as the k^* value increases as the suction-like behavior acts on particles for a cold surface in thermophoresis. This supports the regulation of the heat gradient on the microfluidic scale, which is used in microdevices. Figure 6a–d portrays the influence of Sc on $\chi(\eta)$ for the four different models. An increase in Sc improves $\chi(\eta)$ in all four cases. The ‘‘Schmidt number’’ refers to a dimensionless number that establishes a bond between momentum and mass diffusivities in order to produce a fluid flow. On a more technical level, these two concepts are referred to as the hydrodynamic thickness and mass transportation layers. The value of Sc corresponds to the highest possible concentration. When there is an increase in Sc , an increase in the mass transfer occurs as a result of mass diffusion. The effects of Re_Ω and Re_ω on $G'(0)$ and $F'(0)$ are displayed in Table 3. The effects of Re_Ω , Re_ω , and R on Nu_d and Nu_c are displayed numerically in Table 4. Here, the increase in R improves the heat transfer rate on both surfaces. Moreover, the fluid flow over disk surface shows a better-quality heat transference rate than the fluid flow over the cone surface for an increase in R values. Table 5 displays the effects of Re_Ω , Re_ω , N_t , and k^* on Sh_d and Sh_c . Here, it is clear from the table that the increase in values of N_t and k^* improves Sh_d but decreases Sh_c . Moreover, the fluid flow over the cone surface shows a better-quality mass transference rate than the fluid flow over the disk surface for an increase in the values of N_t and k^* .

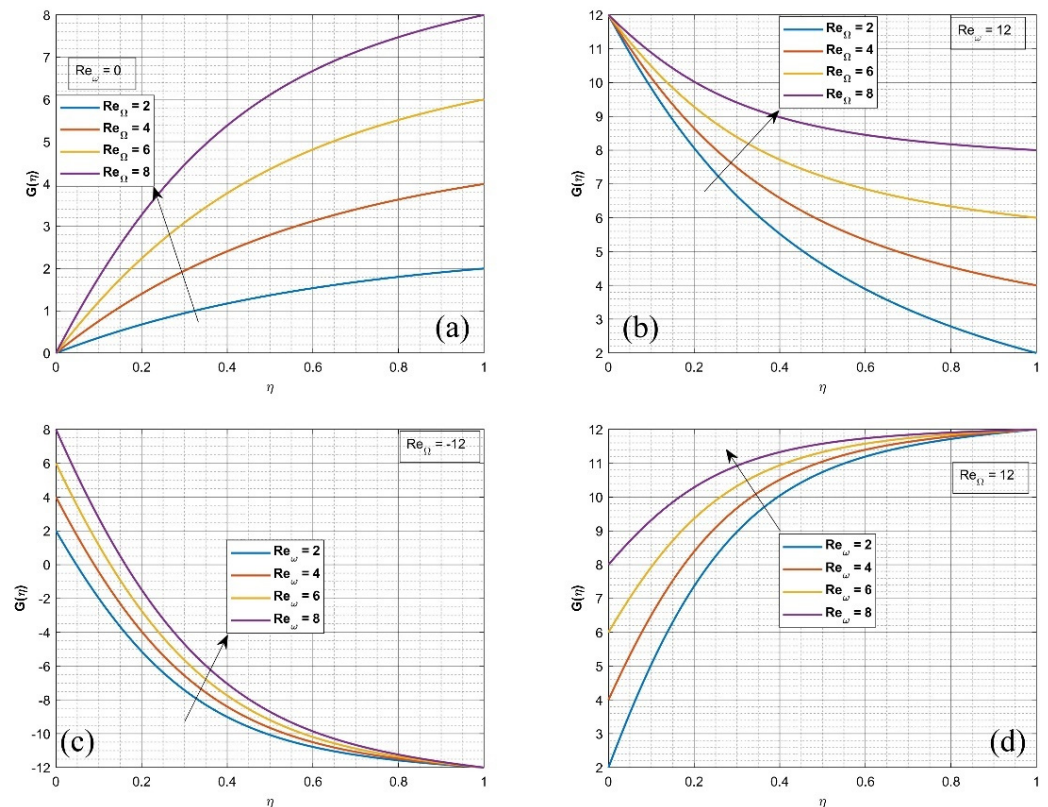


Figure 2. (a–d): The influence of Reynolds numbers on $G(\eta)$; (a) the scenario for the disk at rest and the cone in a revolving state; (b) the variation in Re_Ω on $G(\eta)$; (c) illustrates the scenario for the co-rotation of the disk and cone; (d) the variation in Re_ω on $G(\eta)$.

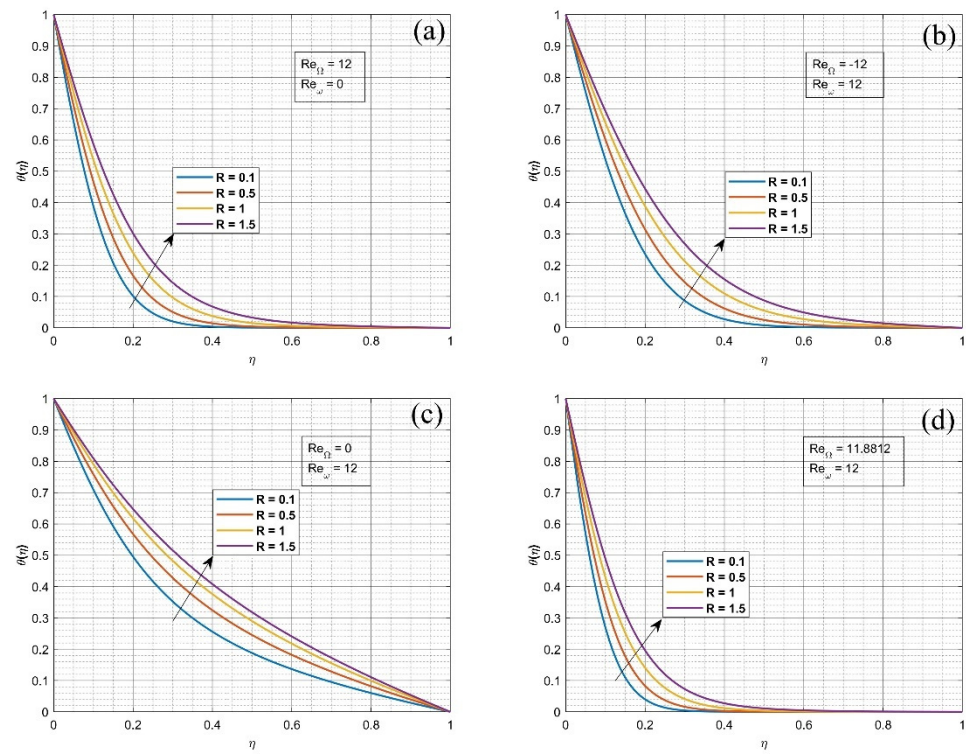


Figure 3. (a–d): Influence of radiation parameter on $\theta(\eta)$ for four different models; (a) the scenario between a rotating cone and stationary disk; (b) the scenario between a counter-rotating cone; (c) the scenario between a rotating disk and a stationary cone; (d) the scenario between a co-rotating cone and disk.

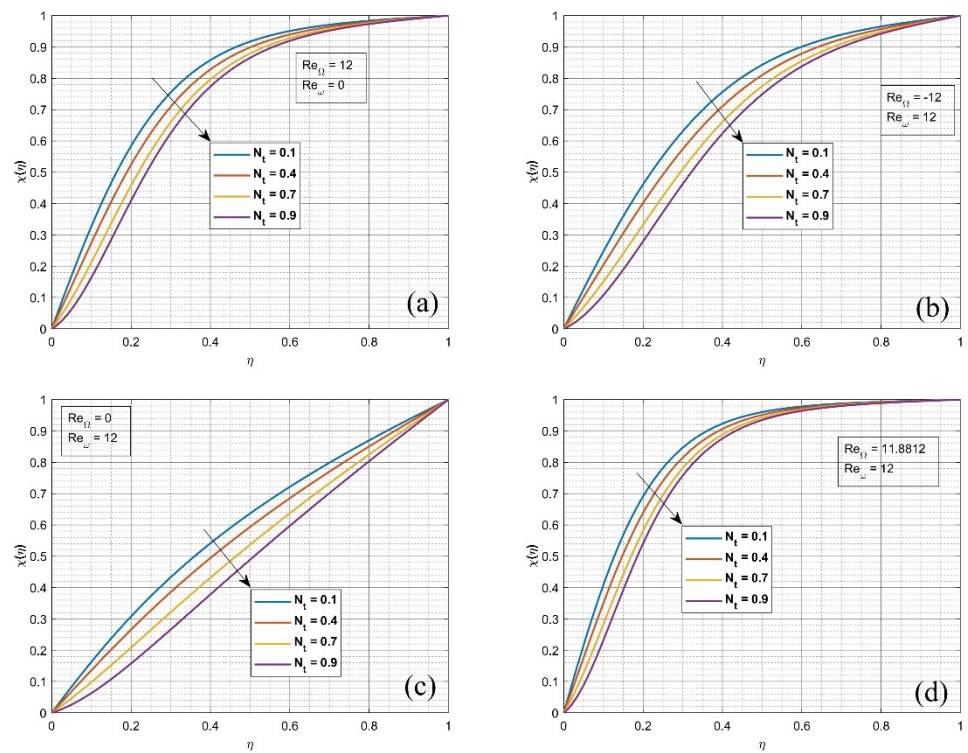


Figure 4. (a–d): Influence of thermophoretic parameter on $\chi(\eta)$; (a) the scenario between a rotating cone and stationary disk; (b) the scenario between a counter-rotating cone; (c) the scenario between a rotating disk and a stationary cone; (d) the scenario between a co-rotating cone and disk.

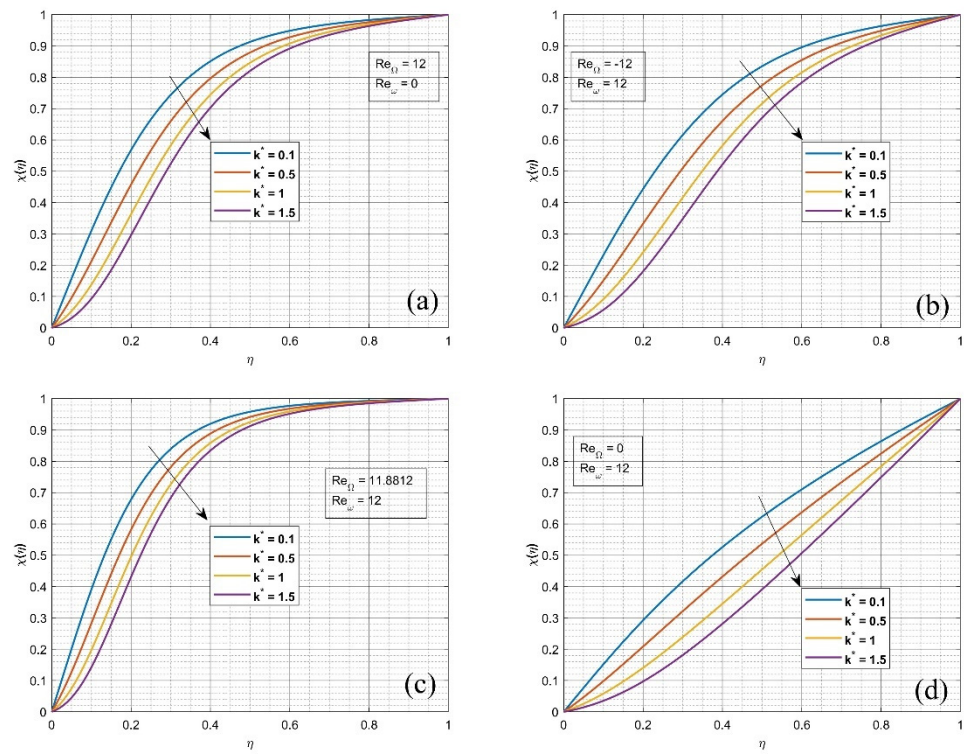


Figure 5. (a–d): Influence of thermophoretic co-efficient on $\chi(\eta)$; (a) is the scenario between a rotating cone and stationary disk; (b) the scenario between a counter-rotating cone; (c) the scenario between a rotating disk and a stationary cone; (d) the scenario between a co-rotating cone and disk.

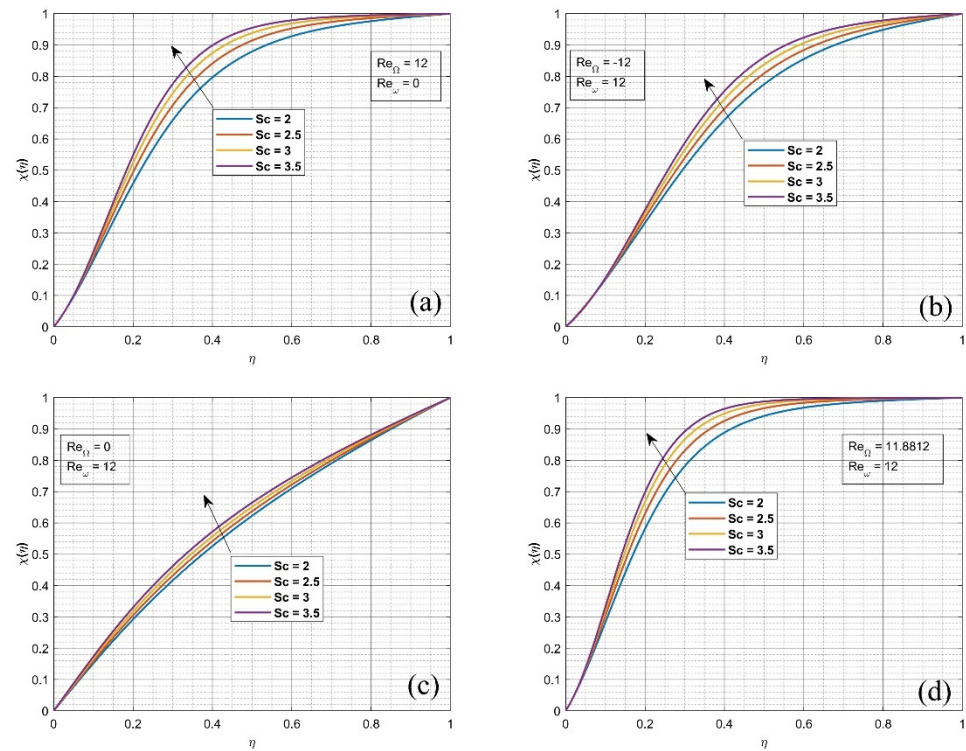


Figure 6. (a–d): Influence of Schmidt number on $\chi(\eta)$; (a) the scenario between a rotating cone and stationary disk; (b) the scenario between a counter-rotating cone; (c) the scenario between a rotating disk and a stationary cone; (d) the scenario between a co-rotating cone and disk.

Table 3. Effects of Re_{Ω} and Re_{ω} on $G'(0)$ and $F'(0)$.

Re_{Ω}	Re_{ω}	$G'(0)$	$F'(0)$
12	11.8812	0.4581	58.104
−12	12	−65.8021	15.2682
0	12	−26.7494	14.3176
12	0	39.1299	35.1944

Table 4. Effects of Re_{Ω} , Re_{ω} , and R on Nu_d and Nu_c .

Re_{Ω}	Re_{ω}	R	Nu_d	Nu_c
2	1	0	1.4871	0.6545
		0.1	1.61348	0.73106
		0.2	1.73988	0.80772
		0.3	1.86641	0.88452
		0.4	1.99304	0.96124
12	11.8812	0.5	11.7474	0.00015
		0.5	6.459	0.01155
		0.5	3.8691	0.5757
		0.5	9.03975	0.00135
		0.5	9.03975	0.00135

Table 5. Effects of Re_{Ω} , Re_{ω} , N_t , and k^* on Sh_d and Sh_c .

Re_{Ω}	Re_{ω}	N_t	k^*	Sh_d	Sh_c
2	1	0.1		−1.2815	−0.767
				−1.2412	−0.7925
				−1.1932	−0.8221
				−1.1356	−0.8564
		0.1		−1.2105	−0.7965
				−1.1135	
				−1.0243	−0.8981
				−0.9422	−0.9483

5. Conclusions

The heat and mass transport characteristics of a liquid flow with TPD across the conical gap of a CDA was analyzed in this study. The disk and cone may be taken as rotating or stationary at varying angular velocities. The Rosseland approximation was used for heat radiation calculations in the current work. To further understand the model’s features, the nonlinear differential equations with associated boundary conditions were solved using the RKF-45 strategy and shooting technique. The main conclusions of the present study are that the fluid particles were aroused by the increasing velocity of both the disk and cone, which is what led to the improvement of the velocity profiles. The velocity profile dramatically increased with increasing values for both cone and disk rotations. The present CDA-type with a radiation effect functioned well in terms of heat transmission. The values of N_t and k^* have a similar qualitative impact on mass transportation for all four models, seeing that the mass transportation decreases as N_t and k^* increase. The fluid flow over the disk surface shows an improved heat transfer rate compared to the fluid flow over cone surface for an increase in R values. The fluid flow over the cone surface shows a better-quality mass transference rate than the fluid flow over the disk surface for an increase in the values of N_t and k^* .

Author Contributions: Conceptualization, H.S., P.S. and S.R.; methodology, B.C.P.; software, H.S.; validation and formal analysis, M.N.; investigation, M.N. and S.R.; resources, B.C.P.; data curation, P.S., M.N. and S.R.; writing—original draft preparation, H.S.; writing—review and editing, B.C.P.; visualization, B.C.P.; supervision, B.C.P.; project administration, B.C.P. All authors have read and agreed to the published version of the manuscript.

Funding: This research received no external funding.

Data Availability Statement: Not applicable.

Conflicts of Interest: The authors declare no conflict of interest.

Nomenclature

R	Radiation parameter	p	Pressure
(r, φ, z)	Cylindrical coordinates (m)	T_w	Temperature of the surface (K)
Nu_d	Nusselt number at the disk's surface	$F(\eta), G(\eta), H(\eta)$	Velocity profiles
T_∞	Ambient temperature (K)	Sc	Schmidt number
k_f	Thermal conductivity ($Wm^{-1}K^{-1}$)	ν_f	Kinematic viscosity of the fluid (m^2s^{-1})
γ	Gap angle	σ^*	Stefan–Boltzmann constant
ϕ	Volume fraction	C	Concentration
T	Temperature (K)	Ψ	Stream function
n	Power index of wall temperature	$\theta(\eta)$	Dimensionless thermal profile
C_∞	Ambient concentration	Re_ω, Re_Ω	Local Reynolds number
ω, Ω	Angular velocities (s^{-1})	k^{**}	Mean absorption coefficient
C_w	Concentration of the surface	U_T and W_T	Thermophoretic velocities (ms^{-1})
(u, v, w)	Constituents of velocity (ms^{-1})	μ	Dynamic viscosity ($kg\ s^{-1}m^{-1}$)
Pr	Prandtl number	k^*	Thermophoretic co-efficient
ρ_f	Density (kgm^{-3})	N_i	Thermophoretic parameter
Nu_c	Nusselt number at cone's surface	$\chi(\eta)$	Dimensionless concentration profile
c	Constant	ρC_{pf}	Heat capacitance

References

- Phan-Thien, N. Cone-and-plate flow of the Oldroyd-B fluid is unstable. *J. Non-Newton. Fluid Mech.* **1985**, *17*, 37–44. [[CrossRef](#)]
- Mooney, M.; Ewart, R.H. The Conicylindrical Viscometer. *Physics* **1934**, *5*, 350–354. [[CrossRef](#)]
- Buschmann, M.H.; Dieterich, P.; Adams, N.A.; Schnittler, H.-J. Analysis of flow in a cone-and-plate apparatus with respect to spatial and temporal effects on endothelial cells. *Biotechnol. Bioeng.* **2005**, *89*, 493–502. [[CrossRef](#)]
- Shevchuk, V. A Self-Similar Solution of Navier–Stokes and Energy Equations for Rotating Flows between a Cone and a Disk. *High Temp.* **2004**, *42*, 104–110. [[CrossRef](#)]
- Basavarajappa, M.; Bhatta, D. Study of flow of Buongiorno nanofluid in a conical gap between a cone and a disk. *Phys. Fluids* **2022**, *34*, 112004. [[CrossRef](#)]
- Wang, F.; Rani, S.P.; Sarada, K.; Gowda, R.P.; Khan, U.; Zahran, H.Y.; Mahmoud, E.E. The effects of nanoparticle aggregation and radiation on the flow of nanofluid between the gap of a disk and cone. *Case Stud. Therm. Eng.* **2022**, *33*, 101930. [[CrossRef](#)]
- Alrabaiah, H.; Bilal, M.; Khan, M.A.; Muhammad, T.; Legas, E.Y. Parametric estimation of gyrotactic microorganism hybrid nanofluid flow between the conical gap of spinning disk-cone apparatus. *Sci. Rep.* **2022**, *12*, 59. [[CrossRef](#)] [[PubMed](#)]
- Gul, T.; Kashifullah; Bilal, M.; Alghamdi, W.; Asjad, M.I.; Abdeljawad, T. Hybrid nanofluid flow within the conical gap between the cone and the surface of a rotating disk. *Sci. Rep.* **2021**, *11*, 1180. [[CrossRef](#)] [[PubMed](#)]
- de Gans, B.-J.; Kita, R.; Wiegand, S.; Luettmmer-Strathmann, J. Unusual Thermal Diffusion in Polymer Solutions. *Phys. Rev. Lett.* **2003**, *91*, 245501. [[CrossRef](#)]
- Podolny, A.; Oron, A.; Nepomnyashchy, A.A. Long-wave Marangoni instability in a binary-liquid layer with deformable interface in the presence of Soret effect: Linear theory. *Phys. Fluids* **2005**, *17*, 104104. [[CrossRef](#)]
- Sarma, R.; Mondal, P.K. Marangoni instability in a viscoelastic binary film with cross-diffusive effect. *J. Fluid Mech.* **2021**, *910*, A30. [[CrossRef](#)]
- Gowda, R.P.; Kumar, R.N.; Aldalbahi, A.; Issakhov, A.; Prasannakumara, B.; Rahimi-Gorji, M.; Rahaman, M. Thermophoretic particle deposition in time-dependent flow of hybrid nanofluid over rotating and vertically upward/ downward moving disk. *Surf. Interfaces* **2021**, *22*, 100864. [[CrossRef](#)]
- Khan, N.S.; Gul, T.; Islam, S.; Khan, W. Thermophoresis and thermal radiation with heat and mass transfer in a magneto-hydrodynamic thin-film second-grade fluid of variable properties past a stretching sheet. *Eur. Phys. J. Plus* **2017**, *132*, 11. [[CrossRef](#)]
- Alhadhrami, A.; Alzahrani, H.A.H.; Kumar, R.N.; Gowda, R.J.P.; Sarada, K.; Prasanna, B.M.; Madhukesh, J.K.; Madhukeshwara, N. Impact of thermophoretic particle deposition on Glauert wall jet slip flow of nanofluid. *Case Stud. Therm. Eng.* **2021**, *28*, 101404. [[CrossRef](#)]
- Abbas, A.; Ashraf, M.; Chamkha, A.J. Combined effects of thermal radiation and thermophoretic motion on mixed convection boundary layer flow. *Alex. Eng. J.* **2021**, *60*, 3243–3252. [[CrossRef](#)]

16. Shah, N.A.; Yook, S.-J.; Tosin, O. Analytic simulation of thermophoretic second grade fluid flow past a vertical surface with variable fluid characteristics and convective heating. *Sci. Rep.* **2022**, *12*, 5445. [[CrossRef](#)]
17. Kármán, T.V. Über laminare und turbulente Reibung. *Z. Angew. Math. Mech.* **1921**, *1*, 233–252. [[CrossRef](#)]
18. Turkyilmazoglu, M. On the fluid flow and heat transfer between a cone and a disk both stationary or rotating. *Math. Comput. Simul.* **2020**, *177*, 329–340. [[CrossRef](#)]
19. Shevchuk, V. Laminar Heat and Mass Transfer in Rotating Cone-and-Plate Devices. *J. Heat Transf.* **2011**, *133*, 024502. [[CrossRef](#)]
20. Tassaddiq, A.; Khan, S.; Bilal, M.; Gul, T.; Mukhtar, S.; Shah, Z.; Bonyah, E. Heat and mass transfer together with hybrid nanofluid flow over a rotating disk. *AIP Adv.* **2020**, *10*, 055317. [[CrossRef](#)]
21. Turkyilmazoglu, M.; Senel, P. Heat and mass transfer of the flow due to a rotating rough and porous disk. *Int. J. Therm. Sci.* **2013**, *63*, 146–158. [[CrossRef](#)]
22. Shevchuk, V. Concerning the effect of radial thermal conductivity in a self-similar solution for rotating cone-disk systems. *Int. J. Numer. Methods Heat Fluid Flow* **2022**, *33*, 204–225. [[CrossRef](#)]
23. Kumar, R.N.; Suresha, S.; Gowda, R.J.P.; Megalamani, S.B.; Prasannakumara, B.C. Exploring the impact of magnetic dipole on the radiative nanofluid flow over a stretching sheet by means of KKL model. *Pramana—J. Phys.* **2021**, *95*, 180. [[CrossRef](#)]
24. Kumar, R.N.; Gamaoun, F.; Abdulrahman, A.; Chohan, J.S.; Gowda, R.J.P. Heat transfer analysis in three-dimensional unsteady magnetic fluid flow of water-based ternary hybrid nanofluid conveying three various shaped nanoparticles: A comparative study. *Int. J. Mod. Phys. B* **2022**, *36*, 2250170. [[CrossRef](#)]
25. Alzahrani, H.A.H.; Alsaiari, A.; Madhukesh, J.K.; Kumar, R.N.; Prasanna, B.M. Effect of thermal radiation on heat transfer in plane wall jet flow of Casson nanofluid with suction subject to a slip boundary condition. *Waves Random Complex Media* **2022**, 1–18. [[CrossRef](#)]
26. Jayaprakash, M.C.; Sarada, K.; Gowda, R.J.P.; Kumar, R.; Fareeduddin, M.; Ibrahim, T.K.; Suresha, S. Three-dimensional unsteady flow of second-grade magnetic nanofluid with KKL correlation model. *Int. J. Mod. Phys. B* **2022**, *36*, 2250188. [[CrossRef](#)]
27. Rahman, M.; Postelnicu, A. Effects of thermophoresis on the forced convective laminar flow of a viscous incompressible fluid over a rotating disk. *Mech. Res. Commun.* **2010**, *37*, 598–603. [[CrossRef](#)]
28. Talbot, L.; Cheng, R.K.; Schefer, R.W.; Willis, D.R. Thermophoresis of particles in a heated boundary layer. *J. Fluid Mech.* **1980**, *101*, 737–758. [[CrossRef](#)]
29. Wang, C. Combined effects of inertial and thermophoresis on particle deposition onto a wafer with wavy surface. *Int. J. Heat Mass Transf.* **2006**, *49*, 1395–1402. [[CrossRef](#)]
30. Chu, Y.-M.; Hashmi, M.S.; Khan, N.; Khan, S.U.; Khan, M.I.; Kadry, S.; Abdelmalek, Z. Thermophoretic particles deposition features in thermally developed flow of Maxwell fluid between two infinite stretched disks. *J. Mater. Res. Technol.* **2020**, *9*, 12889–12898. [[CrossRef](#)]

Disclaimer/Publisher’s Note: The statements, opinions and data contained in all publications are solely those of the individual author(s) and contributor(s) and not of MDPI and/or the editor(s). MDPI and/or the editor(s) disclaim responsibility for any injury to people or property resulting from any ideas, methods, instructions or products referred to in the content.